Research Article | Vol. 28, No. 5 / 2 March 2020 / Optics Express 7408
Optics EXPRESS

Standoff chemical plume detection in turbulent atmospheric conditions with a swept-wavelength external cavity quantum cascade laser

MARK C. PHILLIPS,[1,2,3,*] BRUCE E. BERNACKI,[2] SIVANANDAN S. HARILAL,[2] JEREMY YEAK,[3] AND R. JASON JONES[1]

[1] James C. Wyant College of Optical Sciences, University of Arizona, Tucson, AZ 85721, USA
[2] Pacific Northwest National Laboratory, 902 Battelle Boulevard, Richland, WA 99352, USA
[3] Opticslah, LLC, Albuquerque, NM 87106, USA
[*] mphillips@optics.arizona.edu

Abstract: Rapid and sensitive standoff measurement techniques are needed for detection of trace chemicals in outdoor plume releases, for example from industrial emissions, unintended chemical leaks or spills, burning of biomass materials, or chemical warfare attacks. Here, we present results from 235 m standoff detection of transient plumes for 5 gas-phase chemicals: Freon 152a (1,1-difluoroethane), Freon 134a (1,1,1,2-tetrafluoroethane), methanol (CH_3OH), nitrous oxide (N_2O), and ammonia (NH_3). A swept-wavelength external cavity quantum cascade laser (ECQCL) measures infrared absorption spectra over the range 955-1195 cm^{-1} (8.37- 10.47 μm), from which chemical concentrations are determined via spectral fits. The fast 400 Hz scan rate of the swept-ECQCL enables measurement above the turbulence time-scales, reducing noise and allowing plume fluctuations to be measured. For high-speed plume detection, noise-equivalent column densities of 1-2 ppm*m are demonstrated with 2.5 ms time resolution, improving to 100-400 ppb*m with 100 ms averaging.

1. Introduction

Release of vapor-phase chemicals from localized sources into the atmosphere results in gaseous plumes propagating away from the source; examples may include industrial emissions, unintended chemical leaks or spills, burning of biomass materials, explosive detonations, or a chemical warfare attack. While propagating, these chemical plumes experience dilution and mixing with the atmosphere before eventually reaching equilibrium levels, adsorbing on surfaces, undergoing chemical reactions, or otherwise becoming undetectable. Measurement of a chemical plume near the release point provides valuable information on source concentrations and emission rates, before the plume is subject to atmospheric dilution. For emissions of toxic chemicals where short-term exposure above threshold levels may be acutely harmful or fatal, timely and accurate knowledge of peak concentrations is critical.

Chemical plumes released from localized sources undergo rapid fluctuations in time and space due to atmospheric turbulence. Furthermore, chemical releases may be short-lived in duration leading to highly transient events which need to be detected, for example the gas-phase detonation products generated from an explosive event [1]. Propagation of a plume through the atmosphere is determined by local wind conditions, which vary in time and space due to turbulence. Given that atmospheric turbulence typically occurs on time scales of ~10 ms [2], it is expected that plume dimensions and chemical concentrations may vary on similar time scales, especially near the source release point [3]. Air samples collected near a plume source or further downwind may be analyzed using laboratory methods, but this cannot provide real-time and *in-situ* measurement of plume dynamics and instantaneous concentrations. Passive hyperspectral imaging is useful for

#385850 https://doi.org/10.1364/OE.385850
Journal © 2020 Received 12 Dec 2019; revised 13 Feb 2020; accepted 13 Feb 2020; published 26 Feb 2020

Optics EXPRESS

monitoring plume propagation over large distances and over longer times, and also offers imaging context [4], but high speed and quantitative concentration measurements can be challenging to achieve.

Measuring chemical plumes from a remote distance using active optical standoff detection techniques provides sensitive *in-situ* monitoring of chemical concentrations at or near the source, while keeping equipment and operators at safe distances from the release point. Multiple optical techniques have been applied to standoff chemical detection, especially at ultraviolet (UV), visible (VIS), and near-infrared (NIR) wavelength regions. Differential optical absorption spectroscopy (DOAS) can provide high sensitivity in long-range standoff measurements up to many kilometers, for species with strong absorption in the UV-NIR [5]. Differential absorption LIDAR (DIAL) systems in the VIS-NIR used for remote sensing can measure signals using backscatter from topographic or aerosol targets [6]. NIR wavelength-modulation spectroscopy (WMS) systems have been used for CH_4 and CO_2 detection at 1.3 km standoff [7]. Open-path Fourier transform infrared spectroscopy (OP-FTIR) [8,9] in the NIR has demonstrated outdoor open-path detection at 1.5 km standoff of multiple atmospheric species, with 5 minute measurement times [10]. Frequency comb spectroscopy in the NIR has been applied to standoff detection of atmospheric and greenhouse gases including CH_4, CO_2, and H_2O at distances ~1 km [11–13].

Because standoff detection in the NIR is limited by low absorption cross-sections for most chemical species, many techniques require long averaging times to reduce noise and improve sensitivity. Long averaging times are appropriate for measuring slow atmospheric variations of chemical species occurring over hour-day time periods and may be used to track variations in larger-scale or longer-duration chemical plume releases. However, for measurement of rapid fluctuations in chemical concentrations present in localized and transient chemical plumes, the use of long averaging times is unsuitable, and may reduce the accuracy of the measurement as instantaneous plume concentrations are changed to a time-averaged mean. Furthermore, improvements in signal-to-noise ratio (SNR) are limited to averaging times shorter than the plume duration itself.

To improve sensitivity and reduce the need for averaging, moving to mid-wave infrared (MWIR) wavelengths (3-5 μm) or long-wave infrared (LWIR) wavelengths (8-12 μm) provides advantages by accessing higher molecular absorption cross-sections as well as characteristic fingerprint spectra. Systems using distributed feedback quantum cascade lasers (DFB-QCLs) for standoff detection in the MWIR-LWIR achieve low detection limits for strongly absorbing species at faster measurement times $\lesssim$ 1s [14–17]. However, the small wavelength scanning range of DFB-QCLs limits their use to detection of small molecules with resolved ro-vibrational lines. For detection of larger molecular species, techniques with broad wavelength coverage are required. FTIR provides broad wavelength coverage, but the low spectral radiance of blackbody sources prevents measurement with simultaneous high spectral resolution and fast acquisition speed. With the exception of solar-based atmospheric sounding [18], OP-FTIR in the MWIR or LWIR is usually limited to a few hundred meters. For example, OP-FTIR was used to detect multiple species at 310 m standoff with 1-minute temporal resolution and 0.5 cm^{-1} spectral resolution [19]. Use of laser-based sources with OP-FTIR can improve time-response and spectral resolution. For example, an FTIR-based measurement using an OPO light source was used for indoor standoff detection of methane and ethane at 70 m, with 1 s time resolution and 0.05 cm^{-1} spectral resolution [20]. MWIR dual-comb spectroscopy (DCS) from 3.03-3.64 μm was used for standoff detection at 162 m of acetone and isopropanol vapor with 60 s time resolution, for chemical releases of ~1 hour duration [21]. Even with the higher absorption cross-sections in the MWIR and LWIR spectral regions, achieving simultaneous high-speed and high-sensitivity standoff chemical detection has remained a challenge.

Use of an external cavity quantum cascade laser (ECQCL) provides a combination of broad spectral coverage in the MWIR-LWIR and high spectral resolution, which enables high sensitivity

Optics EXPRESS

detection of multiple chemical species [22]. Despite the advantages afforded by broadly-tunable ECQCL sources for sensitive and high-speed sensing, especially for larger molecules with broad absorption features, there have been only a few reports of their use in standoff detection of chemical plumes [3,23–28]. Swept-wavelength ECQCL systems provide a narrow linewidth laser source which is rapidly tuned across a large infrared tuning range [1,3,28–32]. The broad tuning range (>100 cm^{-1}) in the MWIR-LWIR and fast wavelength sweep rate > 100 Hz provides numerous benefits for standoff detection of multiple chemicals in turbulent environments. A swept-ECQCL system was previously used to perform short-range (10 m) indoor standoff detection of turbulent chemical mixture plumes [3] and measurement of ^{15}N:^{14}N isotope ratios in ammonia [28].

In this paper, we report use of a broadly-tunable swept-ECQCL for simultaneous high-sensitivity and high-speed measurement of transient chemical plumes at a standoff distance of 235 m between the ECQCL and a retro-reflector. A large wavenumber sweep range of 955-1195 cm^{-1} (8.37-10.47 μm) was used to measure 5 gas-phase species – Freon 152a (1,1-difluoroethane), Freon 134a (1,1,1,2-tetrafluoroethane), methanol (CH_3OH), nitrous oxide (N_2O), and ammonia (NH_3). The swept-ECQCL measured infrared absorption spectra over the large tuning range at a rate of 400 Hz, which is shown to be above the frequencies of atmospheric turbulence characterized with the system. The chemicals were released as short-lived gas-phase transient plumes with durations < 60 s, and the fast 400 Hz measurement rate is shown to track variations in plume column densities due to turbulence, allowing accurate measurement of peak values. For all species except N_2O (which has a low absorption cross-section in the wavelength range probed), we demonstrate measurement sensitivities expressed as noise-equivalent column densities (NECD) of 1-2 ppm*m with 2.5 ms time resolution. Averaging for times up to 100 ms improves the NECD to 100-400 ppb*m, with <10% reduction in accuracy for peak concentrations. For detection of changes in slowly-varying chemical sources integrated along the entire measurement path, noise-equivalent concentrations (NECs) of 60-200 ppt are demonstrated for a 10 s averaging time. The ability of the swept-ECQCL system to measure trace concentrations at fast measurement rates provides an important capability for standoff detection of transient chemical plumes.

2. Experimental

Figure 1(a) shows a schematic of the optical layout for the standoff detection system. The output from the swept-ECQCL was a collimated beam with diameter ~3 mm ($1/e^2$). A fraction of the beam was reflected from an uncoated BaF_2 wedged window (WW) and directed to an infrared photodetector DET1 (VIGO PVI-2TE-10.6) for a reference measurement of the ECQCL power before propagation over the long atmospheric path. The beam transmitted through the WW was directed to a beam expander consisting of a negative lens L1 with 25 mm diameter and f=-25 mm (Thorlabs LF7733-F) and a gold-coated 90° off-axis parabolic (OAP) mirror with 75 mm diameter and f=+230 mm (Thorlabs MPD399-M01). The diameter of the expanded launch beam was ~30 mm at the output of the OAP and the divergence of the launch beam was adjusted via translation of L1. The launch beam angle was adjusted using a 102 mm diameter protected silver mirror (Steering Mirror) in a gimbal mount located vertically above the launch OAP, as diagrammed in Fig. 1(b). Return light from the remote target was aligned onto DET2 (VIGO PVI-4TE-10.6) using a second Steering Mirror and OAP, identical to the launch pair. Figure 1(d) shows a photograph of the assembled system in place during the standoff measurements.

The ECQCL standoff system was positioned on the rooftop of a building at the University of Arizona campus. A gold-coated hollow corner cube retro-reflector with 127 mm clear aperture was positioned on the rooftop of a second building. Figure 1(e) indicates the position of the ECQCL standoff system and the retro-reflector on an image obtained from Google Earth. The distance between the standoff system and the retroreflector was 235 m, and the beam was located 18 m above ground level, based on data from Google Earth.

Optics EXPRESS

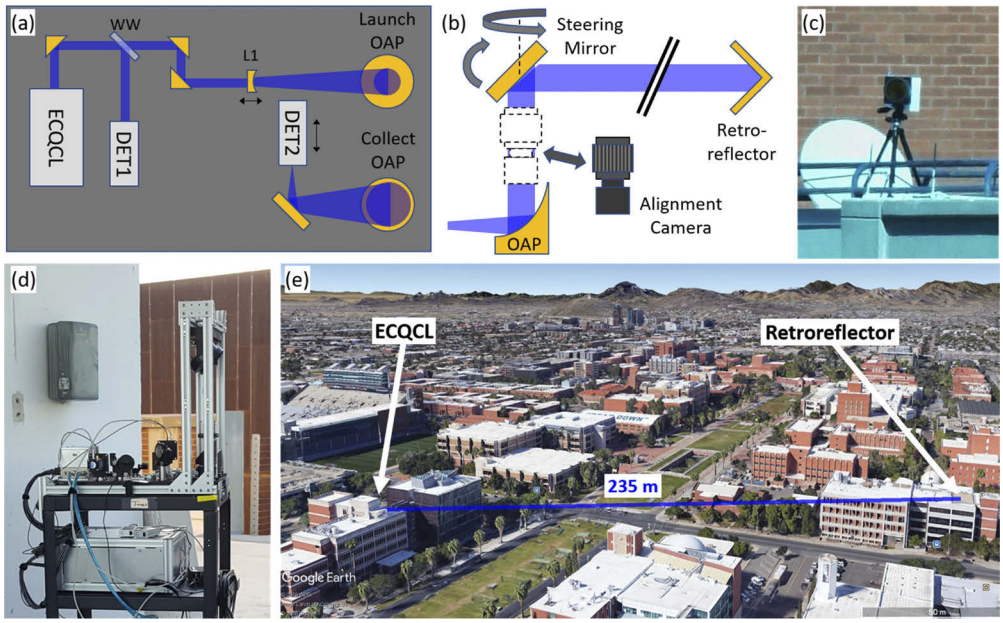

Fig. 1. (a) Schematic of standoff detection optics on 300×600 mm breadboard. (b) Vertical configuration of beam steering optics for alignment of ECQCL beam to a remote retro-reflector target and focusing of return light onto DET2. A visible alignment camera was inserted into the beam path for coarse alignment and removed for measurements with the ECQCL. (c) Image of remote retro-reflector obtained using the alignment camera. (d) Photograph of system in measurement position. (e) Google Earth image of measurement configuration with 235 m standoff distance. Abbreviations: WW – BaF_2 wedged window, L1- Lens, OAP – off-axis parabola, DET1/2 – infrared photodetectors.

Coarse optical alignment of the system was performed by inserting a visible CMOS alignment camera with 45x telescopic lens (Optex Redtail) in the ECQCL beam path between the OAP and steering mirror, as diagramed in Fig. 1(b). The camera was aligned to be co-axial with the ECQCL beam using a close-range target and could be inserted/removed from either beam path using an indexed mechanical mount. The alignment camera was placed in each beam path (launch and collection), and the steering mirror angles were aligned to center the retro-reflector image in the camera field of view. Figure 1(c) shows an image of the remote retro-reflector at 235 m distance taken using the alignment camera (image has been cropped). After adjustment of the steering mirrors in both launch and collection arms, the alignment camera was removed. This initial course alignment procedure produced a signal on DET2 from a portion of the ECQCL light returned from the retro-reflector. Final optimization of the signal was performed by maximizing the signal on DET2 via iteratively adjusting the launch and collection steering mirrors and adjusting the beam divergence via translation of L1.

The custom-built swept-ECQCL was similar to versions reported previously [1,3,28]. The ECQCL used a QCL device (Thorlabs QE) designed for broadband operation in the LWIR and provided an overall tuning range of 910-1215 cm^{-1} (8.23-10.99 μm). For the standoff measurements reported here the tuning range was reduced to 955-1195 cm^{-1} (8.37-10.47 μm). The QCL was operated with amplitude-modulation (AM) of the current from 0-1500 mA using a 500 kHz square wave with 50% duty cycle. The output of the ECQCL had a corresponding full-depth AM in intensity at 500 kHz, enabling lock-in detection of the ECQCL signal in the presence of ambient infrared light on the photodetector. The signals on DET1 and DET2 were

Optics EXPRESS

digitized at a 2 MHz rate using National Instruments hardware and demodulated in software written in LabVIEW, providing measurements of the detected ECQCL intensity at 2 μs intervals.

Scanning of the ECQCL wavenumber was performed using a galvanometer-mounted mirror inside the ECQCL cavity. A 200 Hz sine wave was applied to the galvanometer angle, which provided scanning at a 400 Hz rate (accounting for the forward and backward scans during each cycle of the sine wave). Relative wavenumber calibration was performed by measuring fringes from a solid Si etalon with 0.416 mm thickness (free-spectral range 3.5 cm^{-1}) placed in front of DET1. Calibration of the absolute wavenumber position was performed by comparing a measured absorption spectrum of NH_3 with a spectrum simulated using HITRAN [33]. After calibration, the 400 Hz scan data included a spectral range of 955-1195 cm^{-1} with 0.1 cm^{-1} spacing. Based on the 2.5 ms needed to scan over the 240 cm^{-1} tuning range, the average tuning rate was 96,000 cm^{-1}/s. The average power of the ECQCL over the 400 Hz scan was 3.5 mW and at the peak of the tuning curve (1125 cm^{-1}) the average power was 6.5 mW. At all times, the intensity was below the maximum permissible exposure (MPE) threshold of 100 mW/cm^2 for these infrared wavelengths.

To demonstrate the performance of the system to detect and measure concentrations of chemicals in transient plumes, a sequence of 5 chemicals was released. Plumes of F152a (1,1-difluoroethane), F134a (1,1,1,2-tetrafluoroethane), and N_2O were released directly in the gas-phase from commercial air dusters or gas cartridges. Plumes of methanol (MeOH, 100%) and ammonia (NH_3, 10% aqueous solution) were generated by placing small quantities of liquid on a tissue and allowing the liquid to evaporate. Chemicals were released 1-3 m upwind from the beam path from locations on either building (near the ECQCL system or near the retro-reflector) and no significant difference in results was observed due to the path-integrated measurement configuration. Each chemical release was of short duration <60s, and all the chemicals were released in series over a ~5 min time period.

3. Data acquisition and processing

Multiple data sets were acquired for analysis of the standoff detection performance. To characterize atmospheric turbulence, a data set was acquired with the ECQCL operating at a fixed wavenumber of 965 cm^{-1} and not scanning, providing a continuous measurement of the ECQCL intensity at 2 μs intervals over a duration of several minutes. In scanned operation, the data also consists of a continuous time series of data for the detected ECQCL intensity but modulated in wavenumber at the scan frequency of 400 Hz. After separation of the data stream into individual scans and calibration of the wavenumber axis, each data set is denoted by $I_j(\nu)$ where j denotes the index of the individual scans separated by 2.5 ms time intervals, and ν is the wavenumber.

A data set of 40,000 scans (100 s duration) was used to characterize the background in the absence of any chemical plume releases. A second data set of 100,000 scans (250 s) was used for characterizing the noise and sensitivity of the measurements, also without the plume releases. A third data set was used to measure the series of chemical plumes, which occurred over a ~5 min time period. The scan intensity was converted to absorbance by $A_j(\nu) = -\ln[I_j(\nu)/I_0(\nu)]$ where $I_0(\nu)$ is the average scan intensity for the background data set. Thus, $A_j(\nu)$ measures changes in absorbance relative to the average conditions at the time the background was acquired.

Absorbance spectra were analyzed using a weighted least squares (WLS) algorithm, as has been described previously [3,28–30]. Library absorption spectra for F134a, F152a, and MeOH were obtained from the PNNL/NWIR spectral database [34]. Library absorption spectra for N_2O, NH_3, H_2O, and CO_2 were modeled using parameters from HITRAN [33]. The HITRAN spectra were convolved with a Gaussian function with 0.3 cm^{-1} full width at half maximum (FWHM) to represent an effective instrument function for the ECQCL scan, where the width was determined from minimizing the fit residuals for a measured absorption spectrum. Plots of the library spectra are provided in Fig. 5 in the Results section. The absorbance spectrum baseline was fit using

Optics EXPRESS

additional functions determined from a principal component analysis (PCA) of background data, as will be described in the Results section. The WLS fits were weighted by $I_j(\nu)^2$ to account for increased noise in regions of the spectrum with low detected intensity. The output of the WLS analysis is a time-series of concentrations for each analyzed chemical, at intervals of 2.5 ms. Due to the path-integrated measurement, and because the spatial overlap of the plume with the measurement path is unknown and changing in time, results are reported in units of column density with units of ppm*m or ppb*m. For atmospheric species filling the entire beam path, the column density can be divided by the total measurement path length of 470 m to recover mixing ratios.

4. Results

4.1. Characterization of atmospheric turbulence

Before showing results on plume detection, we first present a characterization of noise due to atmospheric turbulence. For these measurements, the ECQCL was operated at a fixed wavenumber of 965 cm^{-1} without scanning. Figure 2(a) shows a 1 s portion of measured signals on the reference and standoff detectors (DET1 and DET2, respectively) as a function of time. The signal on the reference detector is nearly constant, but the signal on the standoff detector shows fluctuations in amplitude due to effects of propagation over the atmospheric path. The scintillation index σ_I^2 is defined as the normalized variance of the intensity fluctuations $\sigma_I^2 = \langle I^2 \rangle / \langle I^2 \rangle - 1$ [2]. For the data shown in Fig. 2(a), the computed $\sigma_I = 0.13$ would typically be considered weak turbulence, although the peak-to-peak fluctuations of ~70% of the mean are significant when applied to trace gas sensing and detection of small absorbance changes.

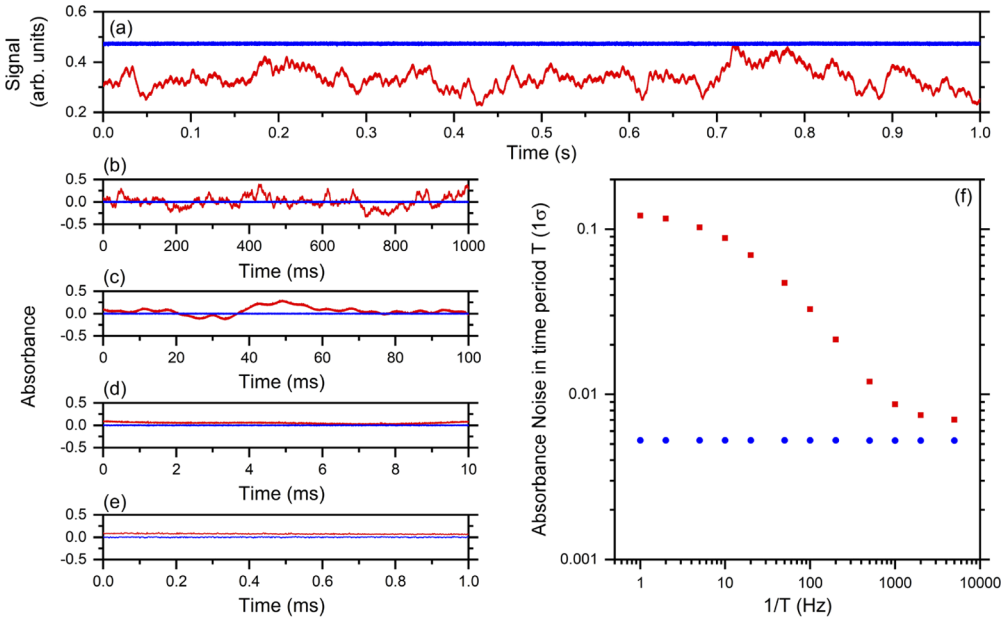

Fig. 2. Effects of atmospheric turbulence on signals recorded by reference detector (DET1, blue) and standoff detector (DET2, red), with the ECQCL at fixed wavenumber of 965 cm^{-1}. (a) Detector signals as function of time. (b)-(d) Absorbance as function of time for decreasing time windows T of (b) 1000 ms, (c) 100 ms, (d) 10 ms, and (e) 1 ms. (f) Absorbance noise (standard deviation of absorbance) over time window T as function of equivalent frequency 1/T.

Optics EXPRESS

Figures 2(b)–2(e) show examples of the temporal intensity fluctuations plotted as absorbance $A(t) = -\ln[I(t)/\langle I(t)\rangle]$, where $\langle I(t)\rangle$ is the mean intensity over the time window plotted. For a scanned system, the time windows would correspond to the time taken to move the wavenumber over a desired scan range. In Fig. 2(b) with a 1 s scan window, and Fig. 2(c) with 100 ms scan window, the absorbance fluctuations severely limit the ability to detect small absorbance features and the fluctuations may be confused with actual chemical absorption spectra. For the smaller scan windows in Figs. 2(d)–2(e) the effective scan time becomes shorter than the characteristic turbulence time scales, leading to a flatter absorbance baseline unrepresentative of absorption from chemical species. Examples of the effects of turbulence on measurement of absorption spectra using a scanned-wavelength system can be found in [3].

Figure 2(f) quantifies the results in terms of absorbance noise (standard deviation of absorbance over the time window of duration T) versus an equivalent frequency 1/T. At slow equivalent frequencies of 1 Hz the absorbance noise is 0.12 and dominated by atmospheric scintillation effects. As the equivalent frequency increases above the frequency scales of turbulence, the absorbance noise decreases by an order of magnitude and approaches the nearly constant value measured from the reference detector. The absorbance noise is slightly lower for the reference detector due to the higher average signal, and we expect the standoff absorbance noise would decrease with higher power on the detector. The results show turbulence time scales ~10 ms, and thus scanning rates > 100 Hz will be beneficial to reduce noise.

4.2. *Correction of swept-ECQCL scan noise*

Figure 3 shows measurements when the swept-ECQCL was scanned at a 400 Hz rate over 955-1195 cm^{-1} (8.37-10.47 μm), for a 200 ms portion of the background data set $I_j(\nu)$ recorded by DET2. The overall shape of $I_j(\nu)$ is determined by the QCL gain profile, ECQCL optics, and detector response. Sharp dips in measured intensity correspond to absorption by atmospheric species, in this case primarily H_2O. The shape of each $I_j(\nu)$ scan in Fig. 3(a) appears similar, other than a scaling in amplitude which varies slowly between the 2.5 ms scan intervals. After conversion to absorbance $A_j(\nu)$, the spectra were found to have a nearly flat baseline with the dominant deviations being variable offsets and slopes, confirming the scan rate is above the dominant turbulence frequency scales. However, the absorbance noise of 0.022 ± 0.007 measured for the 400 Hz scans was higher than the absorbance noise of 0.013 measured for fixed wavenumber operation shown in Fig. 2(f), indicating that the scanning of the swept-ECQCL introduces additional noise into the absorbance spectra.

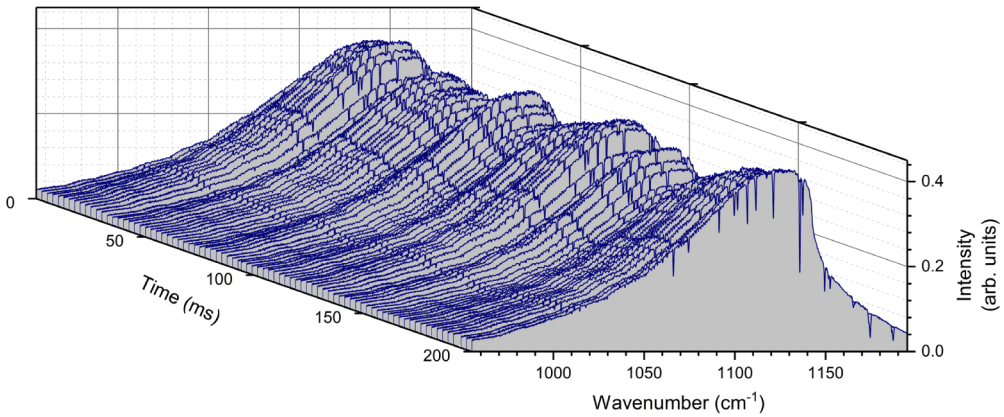

Fig. 3. Measured scan intensity as a function of time for the return signal from retro-reflector, in the absence of chemical plumes. Scans are separated by 2.5 ms.

Optics EXPRESS

To characterize systematic variations in the scan structure, the background data set $I_j(\nu)$ was averaged sequentially over blocks of 200 and absorbance spectra were calculated via $A_j(\nu) = -\ln[I_k(\nu)/I_0(\nu)]$ with $(k = 0 - 200)$. Using the method described in [30], a PCA was performed on the set of background absorbance spectra to characterize the variance in the spectra. Figure 4(a) shows the principal component (PC) scores sorted by decreasing variance. Figure 4(b) shows the first 10 PC vectors, which were found to reproduce the dominant observed scan noise variations, with additional PC vectors characterized by random noise.

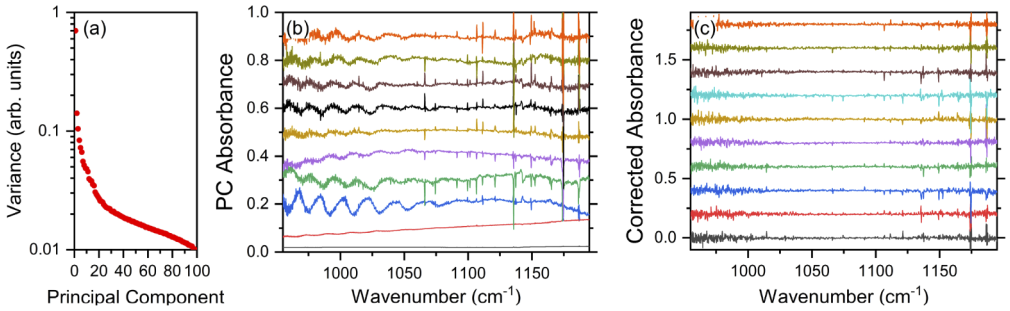

Fig. 4. (a) Principal component analysis (PCA) of background absorbance spectra. (b) First 10 PC vectors (absorbance spectra) from PCA analysis, plotted from bottom to top with decreasing variance, and offset for clarity. (c) Series of 10 absorbance spectra from background data set, after fitting and subtraction of baseline using PC background vectors.

It was shown previously that inclusion of the PC vectors in the analysis library for a WLS spectral analysis significantly reduced the effects of scan noise in a point sensor based on a swept-ECQCL combined with an open-air astigmatic Herriott cell [30]. The PCA analysis of baseline fluctuations is similar in concept to fitting a high-order polynomial to the baseline, but an advantage of the PCA approach is that the baseline is optimized based on measurements of spectral structures present in the absence of chemicals to be detected. In this respect, the data set used in the PCA analysis can be considered a "training set" for the spectral absorbance baseline which is then applied to future data sets. However, it should be noted that any species changing in concentration during the background training set may be included in the PC background vectors and thus these concentrations will not be accurately determined by the WLS algorithm. In the present case, variations in H_2O and higher noise near H_2O absorption lines leads to corresponding structure in the PC background vectors as shown in Fig. 4(b). These structures are highly localized to spectral regions near the H_2O absorption, which are de-weighted in the WLS analysis, and thus have a minimal effect on measurement of other species [30].

Figure 4(c) shows a series of 10 absorbance spectra after fitting of the baseline by including the PC background spectra in the WLS routine. The absorbance noise in the spectra is now reduced to 0.015 ± 0.002, similar to the absorbance noise measured for fixed wavenumber operation at a 400 Hz effective scan rate. The bandwidth normalized absorbance noise for scanned operation at 400 Hz is 5.3×10^{-5} $Hz^{-1/2}$ using a measurement bandwidth of 80 kHz corresponding to the 2 μs point sampling time. If normalized for the total measurement path length of 470 m, the noise-equivalent absorption coefficient is 1.1×10^{-9} $cm^{-1}Hz^{-1/2}$ with no averaging and acquisition time per scan of 2.5 ms.

4.3. *Detection of transient chemical plumes*

Figure 5 shows examples of measured absorbance spectra for each chemical during the plume release experiments, along with the best fit spectra determined from the WLS analysis and the fit residuals. In each case, the absorbance baseline fit by the 10 PC vectors has been subtracted

Optics EXPRESS

and the experimental spectra have been averaged over 100 ms to aid visual comparison with the fitted spectra. Good correspondence is observed between the measured and fit spectra, with low residual structure except near sharp absorption features, and the results are similar to prior laboratory measurements [3,28,29].

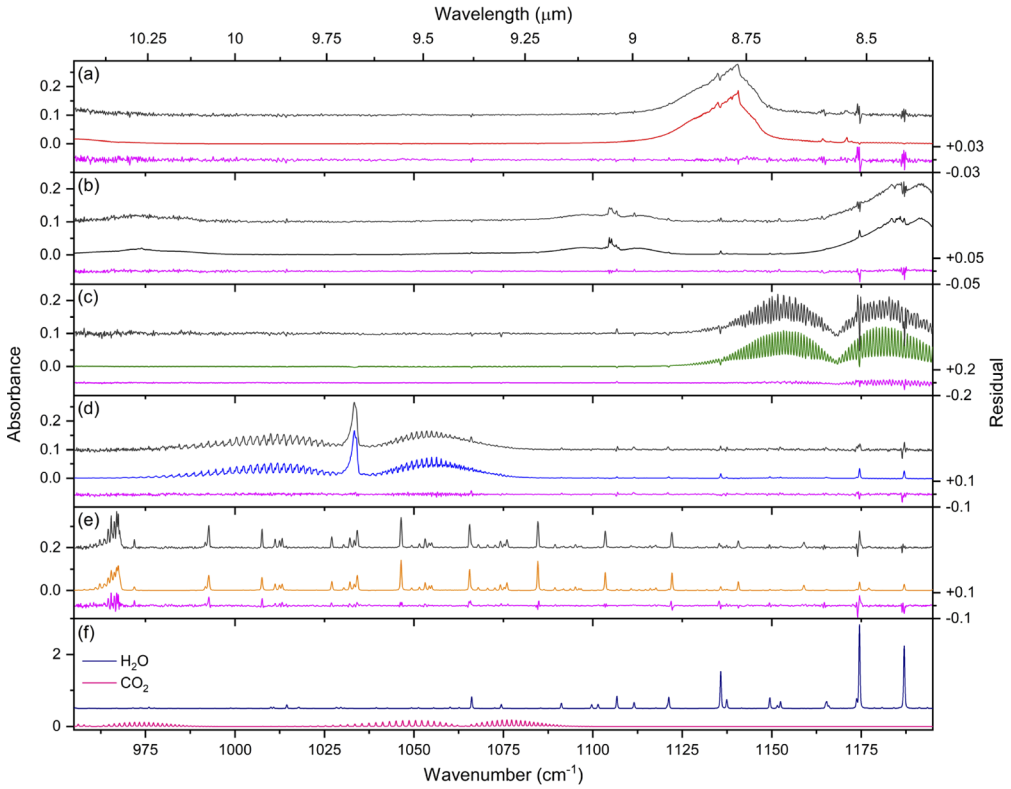

Fig. 5. Absorbance spectra and fits measured during standoff plume detections. In (a)-(f), the top curve is the experimentally measured absorbance spectrum (100 ms average), the middle curve is the best fit spectrum, and the lower curve is the fit residual. (a) F152a, (b) F134a, (c) N_2O, (d) MeOH, and (e) NH_3. Panel (f) shows library absorption spectra for a column density of 10^6 ppm*m H_2O and CO_2.

Figure 6 shows the results of the WLS analysis of all the absorbance spectra acquired during the plume detection experiments. All 5 chemicals were detected above the noise level with good SNR. There is little evidence of cross-talk (false positives) between the different chemicals, except for the region near 13:04:19.05 where the F134a absorbance was very high (>3), corresponding to low detected light levels over a significant portion of the spectrum.

Figure 7 highlights the reduction in noise by including the PC background vectors in the analysis library. When the PC background vectors are not included in the analysis library, the peak N_2O signals shown in Fig. 7(a) are low compared to the noise and the smaller secondary peak at 13:05:00-13:05:05 is not visible. Inclusion of the PC background vectors reduces the noise significantly, allowing smaller peaks to be detected with confidence. The results shown in Fig. 7(b) for MeOH confirm that the inclusion of the PC background vectors does not reduce the accuracy of the measurements significantly, since the magnitude of the MeOH column density is similar in both cases. However, inclusion of the PC vectors reduces the effects of scan noise on the retrieved concentration values, both with and without an absorbing chemical present.

Optics EXPRESS

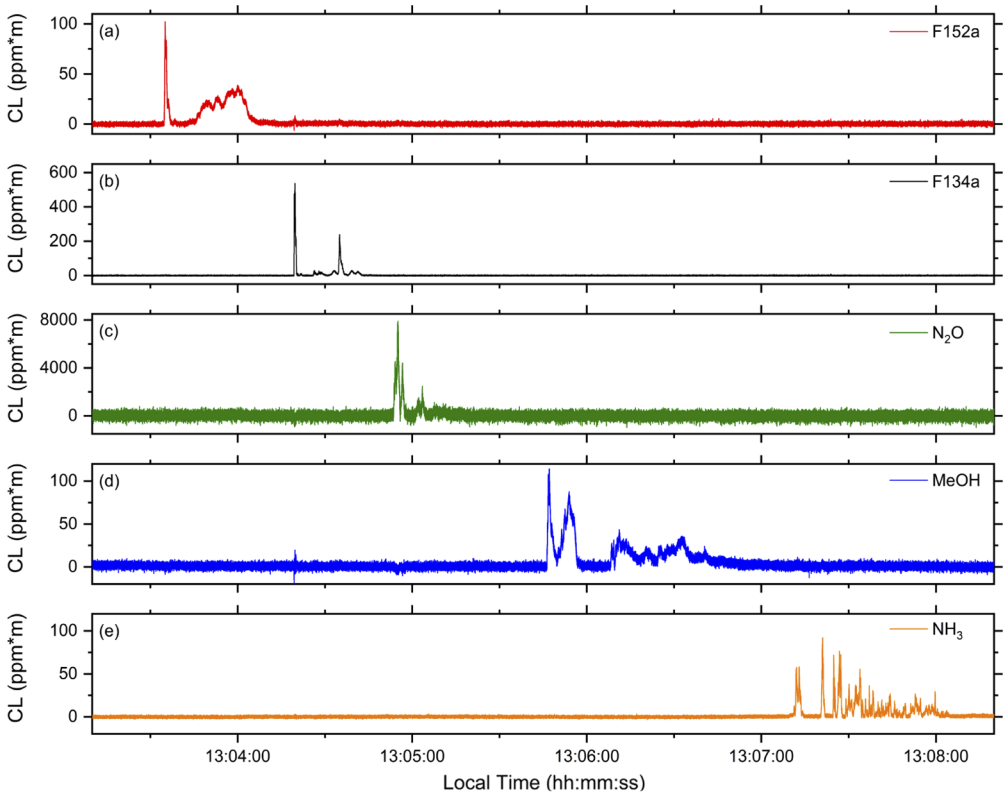

Fig. 6. Detected column density CL (units of ppm*m) versus time for (a) F152a, (b) F134a, (c) N_2O, (d) MeOH, and (e) NH_3 in standoff plume detection experiment.

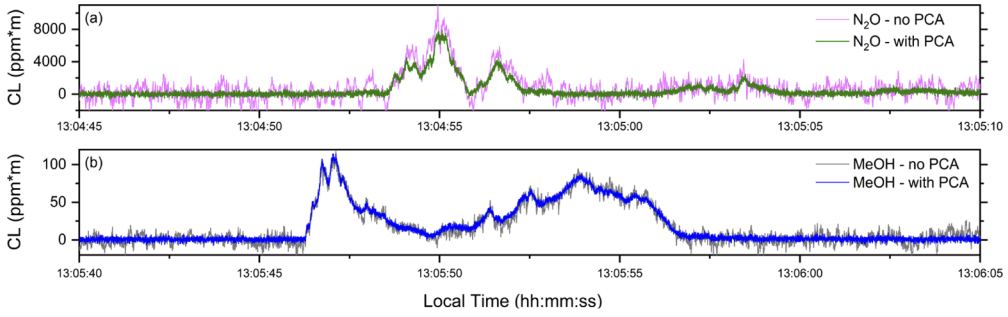

Fig. 7. Measured (a) N_2O, and (b) MeOH signals versus time with and without inclusion of the PC background vectors in the analysis library to fit the absorbance baseline.

Optics EXPRESS

While having a fast scan rate is critical for reducing noise, it is also important to have a fast measurement rate for tracking variations in plume concentrations. Figure 8 shows the column density versus time for NH_3 at the swept-ECQCL measurement rate of 400 Hz (2.5 ms intervals) versus the results when the spectra are first averaged to 1 Hz before the WLS analysis. At the 1 Hz measurement rate, the fast plume variations are not captured, and the peak measured values are in many cases < 50% of the values measured at the 400 Hz rate. The actual plume fluctuations occur on time scales < 100 ms, as shown in the inset, and the turbulent source leads to nearly 100% variations in signals over these time scales. The inset also clearly shows that the noise of the swept-ECQCL measurement at 400 Hz is much lower than the signal variations in the plume.

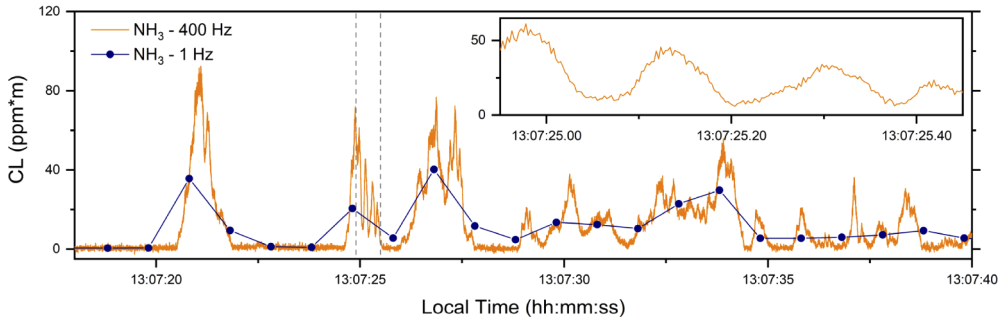

Fig. 8. Effect of measurement rate on retrieved column density of NH_3. The solid line shows retrieved values for analysis of scan acquired at a 400 Hz rate. The circles show retrieved values when scans are pre-averaged to a 1 Hz rate before analysis. The inset shows a zoom of a 500 ms region between the dashed vertical lines.

Noise-equivalent detection sensitivities were evaluated using statistical analysis of repeated measurements without a chemical plume present. The WLS analysis was performed on a background data set of 100,000 scans acquired over a 250 s time period with no plumes present. This background data set was different from the training set used for the PCA background analysis. Figure 9 shows the results of an Allan-Werle analysis [35] on the column density values determined from the WLS analysis of the background data set, which shows the noise-equivalent column density (NECD) as a function of averaging time for each chemical [29]. Figure 9(a) shows the results when the PC background vectors are included in the analysis library and for reference Fig. 9(b) shows results when the PC background vectors are not included. The results again confirm that the PC background vectors remove noise in the output concentrations and allow averaging over longer time periods to reduce noise.

The NECD plotted in Fig. 9 scales with the peak absorption cross-section for each species, as expected. In particular, N_2O has a relatively weak cross-section in the wavelength range probed and thus has a higher noise in the detected column density. For all species except NH_3, the NECD continues to improve with averaging beyond 10 s. In the case of NH_3, there is a rise after 1 s likely due to real changes in NH_3 concentrations over the measurement path length during acquisition of the background data set. At 1s averaging time and over the total measurement path length of 470 m, the NECD corresponds to 100 ppt NH_3. Given that ambient concentrations of NH_3 are often in the ppb-range and can exhibit local variations due to biogenic and non-biogenic sources [36], it would not be unexpected to observe changes at the 100 ppt level.

For detection of constant or slowly varying sources, the Allan deviation is usually sufficient to characterize the improvement in sensitivity with increasing averaging times. It is clear from Fig. 9 that averaging leads to a reduction in measurement noise levels. However, for detection of transient sources such as plumes, the peak detected signals may also decrease with averaging, leading to a reduction in SNR.

Optics EXPRESS

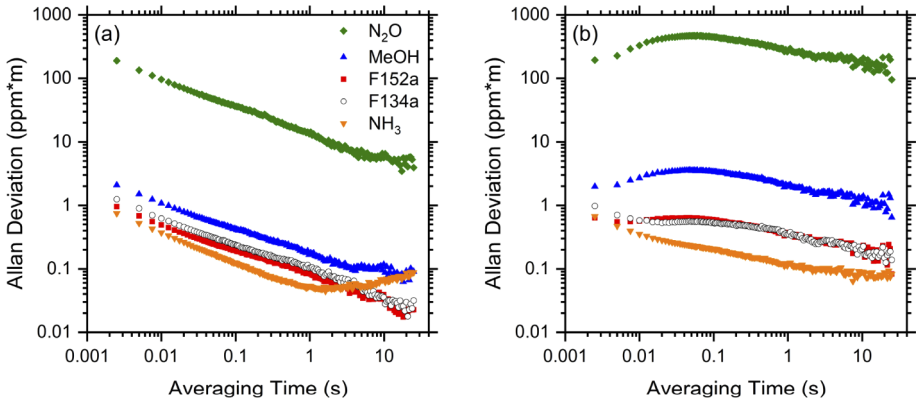

Fig. 9. Allan deviation analysis of background data set with 100,000 measurements (a) with and (b) without inclusion of PC background vectors in analysis library. Results are shown for N_2O (green diamonds), MeOH (blue triangles), F152a (red squares), F134a (black open circles), and NH_3 (orange inverted triangles).

To characterize the SNR for plume detection, the measured column densities shown in Fig. 6 were averaged over different time scales and the peak signal levels were determined. Figure 10(a) shows the peak detected column density for the plume measurements as a function of averaging time, as a percentage of the maximum column density measured with no averaging. As expected, the peak column density decreases with averaging, similar to the results shown in Fig. 8. For averaging times up to ~100 ms the peak column density is reduced by <10%, because the plume fluctuations occur primarily over longer time scales. For averaging times above ~100 ms, the peak detected column density decreases rapidly. Figure 10(b) shows the plume SNR calculated by dividing the peak column density by the Allan deviation at each averaging time. The absolute values of SNR depend on the strength of plume releases and are not particularly significant here. However, we observe that for all species except MeOH, the SNR decreases after ~1s due to the finite duration of the plumes. For MeOH, the SNR does not decrease because the plume duration is longer than the other species, as can be seen in Fig. 6.

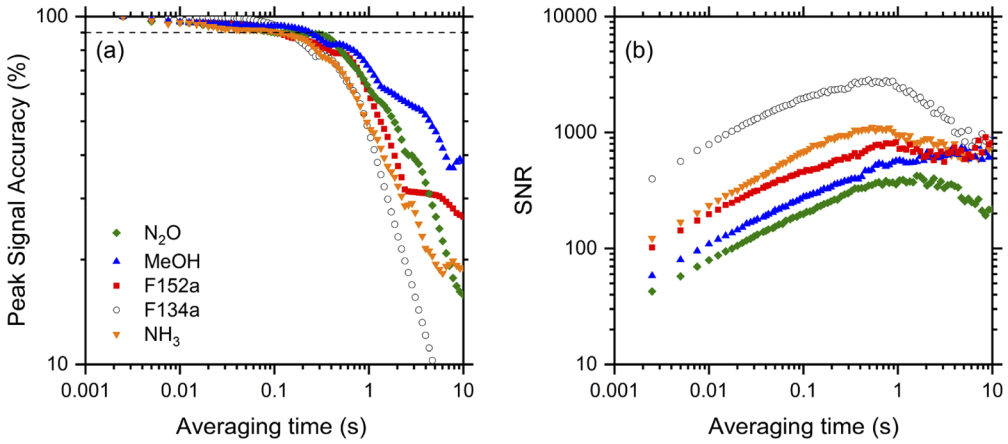

Fig. 10. Effects of averaging on plume detection for (a) peak column density and (b) signal-to-noise ratio (SNR). Results are shown for N_2O (green diamonds), MeOH (blue triangles), F152a (red squares), F134a (black open circles), and NH_3 (orange inverted triangles).

Optics EXPRESS

For the chemical plumes measured in these experiments, we propose an optimal averaging time of 100 ms. For this averaging time, the SNR improves by ~10× relative to a 2.5 ms measurement time, while preserving the peak signal levels to within 90% of the values measured at 2.5 ms. For other chemical plume detection applications, the optimum averaging time will change depending on the time scales of the releases and tolerable reductions in accuracy for peak values. Nevertheless, the results clearly show the importance of fast measurement speed and the limitations of long signal averaging for detection of transient sources.

5. Discussion

Table 1 summarizes the results on NECD, obtained from the Allan deviation analysis in Fig. 9(a). At the fastest measurement time of 2.5 ms, the NECD is ~1-2 ppm*m for all species except N_2O. As noted previously, the N_2O absorption bands are weak in the wavelength range probed by the swept-ECQCL, and better sensitivity has been obtained by measuring at other wavelengths [1]. For the optimum plume averaging time of 100 ms, the NECD improves to 100-400 ppb*m. For a plume of known size L along the measurement path, the results can be multiplied by 1/2L to determine the minimum change in average plume concentration which can be detected, expressed as a noise-equivalent concentration (NEC). For example, a NH_3 plume with 10 m depth has a NEC of 6 ppb at 100 ms averaging time.

Table 1. Noise-equivalent column density (NECD) and noise-equivalent concentration (NEC) for 235 m standoff detection using swept-ECQCL. Plume NECD is in units of column density (ppm*m) for a plume of unknown size. Full path NEC is in units of ppb, assuming a uniform species distribution along entire measurement path length of 470 m.

Species	Plume NECD (ppm*m)	Plume NECD (ppm*m)	Full path NEC (ppb)	Full path NEC (ppb)
	2.5 ms	***100 ms***	***2.5 ms***	***10 s***
F152a	0.96	0.19	2.0	0.062
F134a	1.3	0.23	2.7	0.060
MeOH	2.1	0.41	4.5	0.19
NH_3	0.75	0.12	1.6	0.13
N_2O	191	36	406	14

In addition to detection of localized plumes passing through the measurement path, the results can also be applied for measuring changes in average concentrations for species uniformly distributed along the entire 470 m path length. In this case, NECs are < 5 ppb when measuring at the fastest rate of 2.5 ms. Measurements at high rates such as this may be useful for flux measurements and eddy covariance [37]. For measurements of slowly-varying trace species over the full beam path, Table 1 also shows the NEC at 10 s averaging time. In this case, the NEC ranges from 60-190 ppt. As noted above, determination of the NEC for NH_3 was likely degraded due to variation in ambient NH_3 concentration during the acquisition of the background data set used in the Allan-Werle analysis.

A direct and quantitative comparison of NECD to other standoff detection techniques is not practical due to differences in detected species, and large variations in absorption cross-section with wavelength; nevertheless, some qualitative comparisons are possible. The swept-ECQCL results are comparable or better to many reported measurements using DFB-QCLs for standoff detection in the MIR, where reported NECDs are typically ~1 ppm*m $Hz^{-1/2}$ for strongly absorbing species [14–17]. A NIR WMS system was used for detection of CH_4 and CO_2 at 1.3 km standoff, with sensitivity of 100 ppb (260 ppm*m) for CH_4 at 1 s and 20 ppb (50 ppm*m) at 60 s [7]. DIAL measurements based on broadening of a NIR external cavity diode laser using an electro-optic modulator was used for detection of CO_2, CH_4, and H_2O in an integrated-path

Optics EXPRESS

configuration at 2.75 km standoff, showing a 100 ppb sensitivity for CH_4 at 1 s (550 ppm*m), and improving to 7 ppb (40 ppm*m) with 1000 s of averaging [6].

The results from the swept-ECQCL measurements using the 470 m total beam path and 10 s averaging indicate that many trace species may be detected at <200 ppt concentrations, which is comparable to sensitivities obtained using DOAS at longer path lengths and longer integration times. For example, NO_2 was detected using DOAS with a sensitivity of 60 ppt over a total path length of 5.7 km but used a long averaging time of 30 min [5]. The swept-ECQCL Allan deviation results in Fig. 9(a) also indicate that sensitivity may improve further with additional averaging.

The swept-ECQCL also achieves high sensitivity at fast measurement rates, which is important for measurement of transient events such as chemical plumes. NECDs obtained with the swept-ECQCL were shown to be 1-2 ppm*m for many species at a fast measurement time of 2.5 ms. Recent results using NIR DCS for standoff detection have reported similar sensitivities but only with averaging for hundreds of seconds [11,12]. Standoff measurements using MIR DCS at 3.03-3.64 μm accessed stronger absorption cross-sections for detection of broadband absorbing species acetone and isopropanol, and reported sensitivities of 2-6 ppm*m, with a 60 s averaging time [21]. The closest comparable frequency comb result used a laser centered at 3.25 μm combined with a virtual-image phased array (VIPA) spectrometer for standoff detection of CH_4 and reported a sensitivity of 230 ppb*m*$Hz^{-1/2}$ corresponding to ~5 ppm*m at the fastest measurement time of 2 ms, capitalizing on the high MIR cross-section and use of a multi-channel array detector [38].

6. Conclusions

Achieving high sensitivity in practical sensing conditions often requires optimization of the experiment and analysis to reduce the effects of the frequency-dependent noise. In broadband spectroscopy techniques, noise and structure in the absorbance baseline often limits sensitivity or leads to false detections if baseline structure appears similar to real molecular absorption features. In the case of a scanned-wavelength system such as the swept-ECQCL system used here, temporal fluctuations in intensity are mapped directly into spectral fluctuations, thus it is critical to understand the temporal characteristics of both noise and signals.

Characterization of atmospheric turbulence at the measurement location showed that absorbance noise was reduced through scanning of the wavelength at a 400 Hz rate, above the dominant frequencies of atmospheric turbulence. Systematic structure in the baseline related to the ECQCL scan was removed by performing a PCA analysis of a background training set and using the analysis results as basis vectors to fit the absorbance baseline in analysis of subsequent spectra. We estimate that the combination of these two steps resulted in at least an order-of-magnitude improvement in sensitivity.

Detection of transient chemical plumes in the atmosphere places additional requirements on the sensor's temporal response. Measurement of absorption spectra using the swept-ECQCL at a 400 Hz rate allowed tracking of the variations in column densities occurring on <100 ms time scales. Averaging of column densities up to 100 ms was shown to improve sensitivity with <10% reduction in peak values but averaging for longer times resulted in significant errors in the peak column density levels. Furthermore, the SNR was shown to decrease for averaging times > 1 s due to the finite duration of the plumes, even though the NECD continued to improve for longer averaging times. The results show that for accurate measurement of peak concentrations in chemical plumes in outdoor turbulent environments, a fast measurement rate is essential. Depending on the application, it may be necessary to limit the averaging time due to requirements on accuracy for determining time-resolved release rates. There may also be requirements driven by safety, if detecting chemicals which are acutely toxic above a given threshold concentration.

Optics EXPRESS

In summary, we used a swept-ECQCL source to demonstrate detection of multiple chemicals in outdoor plume releases using a 235 m standoff distance to a retro-reflector. The broad tuning range of the swept-ECQCL from 955-1195 cm^{-1} (8.37-10.47 μm) allowed measurement of many chemical species in the molecular fingerprint region. For the experiments presented here 5 chemicals were selected and the results can be readily extended to additional molecular species. Measurement of spectra using the swept-ECQCL at a 400 Hz rate allowed tracking of the variations in chemical column densities. NECDs of ~1-2 ppm*m were demonstrated using a 2.5 ms measurement time, improving to 100-400 ppb*m with averaging to 100 ms. For detection of slowly varying gases filling the entire measurement path, NECs are predicted to be 60-190 ppt, and the ability of the swept-ECQCL system to detect multiple trace gases at ppt-scale concentrations in open-path configurations may be useful for applications for atmospheric sensing and research.

Funding

Department of Energy Small Business Innovative Research and Small Business Technology Transfer (DE-SC0019855); Office of Defense Nuclear Nonproliferation.

Acknowledgments

We thank Caroline Lecaplain, Yu Zhang, Reagan R. D. Weeks, and Ryan Rhoades for assistance during the plume measurements. The Pacific Northwest National Laboratory is operated for the U.S. Department of Energy (DOE) by the Battelle Memorial Institute under Contract No. DE-AC05-76RL01830.

Disclosures

MCP: Opticslah, LLC (E). JY: Opticslah, LLC (I, E).

References

1. M. Phillips, B. Bernacki, S. Harilal, B. Brumfield, J. Schwallier, and N. Glumac, "Characterization of High-Explosive Detonations using Broadband Infrared ECQCL Absorption Spectroscopy," J. Appl. Phys. **126**(9), 093102 (2019).
2. L. C. Andrews, R. L. Phillips, and C. Y. Hopen, *Laser Beam Scintillation with Applications* (SPIE, 2001).
3. M. C. Phillips and B. E. Brumfield, "Standoff detection of turbulent chemical mixture plumes using a swept external cavity quantum cascade laser," Opt. Eng. **57**(1), 011003 (2017).
4. M. Ghandehari, M. Aghamohamadnia, G. Dobler, A. Karpf, K. Buckland, J. Qian, and S. Koonin, "Mapping Refrigerant Gases in the New York City Skyline," Sci. Rep. **7**(1), 2735 (2017).
5. J.-M. Nasse, P. G. Eger, D. Poehler, S. Schmitt, U. Friess, and U. Platt, "Recent improvements of long-path DOAS measurements: impact on accuracy and stability of short-term and automated long-term observations," Atmos. Meas. Tech. **12**(8), 4149–4169 (2019).
6. G. A. Wagner and D. F. Plusquellic, "Ground-based, integrated path differential absorption LIDAR measurement of CO2, CH4, and H2O near 1.6 mu m," Appl. Opt. **55**(23), 6292–6310 (2016).
7. J. Xia, F. Zhu, S. Zhang, A. Kolomenskii, J. Dong, K. Okada, J. Strohaber, and H. A. Schuessler, "Probing greenhouse gases in turbulent atmosphere by long-range open-path wavelength modulation spectroscopy," Opt. Laser. Eng. **117**, 21–28 (2019).
8. R. J. Yokelson, D. W. T. Griffith, and D. E. Ward, "Open-path Fourier transform infrared studies of large-scale laboratory biomass fires," J. Geophys. Res.: Atmos. **101**(D15), 21067–21080 (1996).
9. Z. Bacsik, J. Mink, and G. Keresztury, "FTIR spectroscopy of the atmosphere. I. Principles and methods," Appl. Spectrosc. Rev. **39**(3), 295–363 (2004).
10. D. W. T. Griffith, D. Pohler, S. Schmitt, S. Hammer, S. N. Vardag, and U. Platt, "Long open-path measurements of greenhouse gases in air using near-infrared Fourier transform spectroscopy," Atmos. Meas. Tech. **11**(3), 1549–1563 (2018).
11. G. B. Rieker, F. R. Giorgetta, W. C. Swann, J. Kofler, A. M. Zolot, L. C. Sinclair, E. Baumann, C. Cromer, G. Petron, C. Sweeney, P. P. Tans, I. Coddington, and N. R. Newbury, "Frequency-comb-based remote sensing of greenhouse gases over kilometer air paths," Optica **1**(5), 290–298 (2014).
12. S. Coburn, C. B. Alden, R. Wright, K. Cossel, E. Baumann, G. W. Truong, F. Giorgetta, C. Sweeney, N. R. Newbury, K. Prasad, I. Coddington, and G. B. Rieker, "Regional trace-gas source attribution using a field-deployed dual frequency comb spectrometer," Optica **5**(4), 320–327 (2018).

Optics EXPRESS

13. K. C. Cossel, E. M. Waxman, F. R. Giorgetta, M. Cermak, I. R. Coddington, D. Hesselius, S. Ruben, W. C. Swann, G. W. Truong, G. B. Rieker, and N. R. Newbury, "Open-path dual-comb spectroscopy to an airborne retroreflector," Optica **4**(7), 724–728 (2017).
14. A. Diaz, B. Thomas, P. Castillo, B. Gross, and F. Moshary, "Active standoff detection of CH4 and N2O leaks using hard-target backscattered light using an open-path quantum cascade laser sensor," Appl. Phys. B: Lasers Opt. **122**(5), 121 (2016).
15. M. Nikodem and G. Wysocki, "Chirped Laser Dispersion Spectroscopy for Remote Open-Path Trace-Gas Sensing," Sensors **12**(12), 16466–16481 (2012).
16. N. S. Daghestani, R. Brownsword, and D. Weidmann, "Analysis and demonstration of atmospheric methane monitoring by mid-infrared open-path chirped laser dispersion spectroscopy," Opt. Express **22**(S7), A1731–A1743 (2014).
17. N. A. Macleod, R. Rose, and D. Weidmann, "Middle infrared active coherent laser spectrometer for standoff detection of chemicals," Opt. Lett. **38**(19), 3708–3711 (2013).
18. A. Kuze, H. Suto, M. Nakajima, and T. Hamazaki, "Thermal and near infrared sensor for carbon observation Fourier-transform spectrometer on the Greenhouse Gases Observing Satellite for greenhouse gases monitoring," Appl. Opt. **48**(35), 6716–6733 (2009).
19. Y. You, R. M. Staebler, S. G. Moussa, Y. Su, T. Munoz, C. Stroud, J. Zhang, and M. D. Moran, "Long-path measurements of pollutants and micrometeorology over Highway 401 in Toronto," Atmos. Chem. Phys. **17**(22), 14119–14143 (2017).
20. O. Kara, F. Sweeney, M. Rutkauskas, C. Farrell, C. G. Leburn, and D. T. Reid, "Open-path multi-species remote sensing with a broadband optical parametric oscillator," Opt. Express **27**(15), 21358–21366 (2019).
21. G. Ycas, F. R. Giorgetta, K. C. Cossel, E. M. Waxman, E. Baumann, N. R. Newbury, and I. Coddington, "Mid-infrared dual-comb spectroscopy of volatile organic compounds across long open-air paths," Optica **6**(2), 165–168 (2019).
22. A. Hugi, R. Maulini, and J. Faist, "External cavity quantum cascade laser," Semicond. Sci. Technol. **25**(8), 083001 (2010).
23. A. K. Goyal, P. Kotidis, E. R. Deutsch, N. Zhu, M. Norman, J. Ye, K. Zafiriou, and A. Mazurenko, "Detection of chemical clouds using widely tunable quantum cascade lasers," Proc. SPIE **9455**, 94550L (2015).
24. A. P. M. Michel, P. Q. Liu, J. K. Yeung, P. Corrigan, M. L. Baeck, Z. Wang, T. Day, F. Moshary, C. F. Gmachl, and J. A. Smith, "Quantum cascade laser open-path system for remote sensing of trace gases in Beijing, China," Opt. Eng. **49**(11), 111125 (2010).
25. R. Aharoni, I. Ron, N. Gilad, A. Manor, Y. Arav, and S. Kendler, "Real-time stand-off spatial detection and identification of gases and vapor using external-cavity quantum cascade laser open-path spectrometer," Opt. Eng. **54**(6), 067103 (2015).
26. N. A. Macleod, F. Molero, and D. Weidmann, "Broadband standoff detection of large molecules by mid-infrared active coherent laser spectrometry," Opt. Express **23**(2), 912–928 (2015).
27. N. A. Macleod and D. Weidmann, "High sensitivity stand-off detection and quantification of chemical mixtures using an Active Coherent Laser Spectrometer (ACLaS)," Proc. SPIE **9824**, 98240B (2016).
28. M. C. Phillips, B. E. Brumfield, and S. S. Harilal, "Real-time standoff detection of nitrogen isotopes in ammonia plumes using a swept external cavity quantum cascade laser," Opt. Lett. **43**(17), 4065–4068 (2018).
29. B. E. Brumfield, M. S. Taubman, J. D. Suter, and M. C. Phillips, "Characterization of a swept external cavity quantum cascade laser for rapid broadband spectroscopy and sensing," Opt. Express **23**(20), 25553–25569 (2015).
30. M. C. Phillips, M. S. Taubman, B. E. Bernacki, B. D. Cannon, R. D. Stahl, J. T. Schiffern, and T. L. Myers, "Real-time trace gas sensing of fluorocarbons using a swept-wavelength external cavity quantum cascade laser," Analyst **139**(9), 2047–2056 (2014).
31. B. E. Brumfield, M. S. Taubman, and M. C. Phillips, "Rapid and Sensitive Quantification of Isotopic Mixtures Using a Rapidly-Swept External Cavity Quantum Cascade Laser," Photonics **3**(2), 33 (2016).
32. B. E. Brumfield and M. C. Phillips, "Quantitative isotopic measurements of gas-phase alcohol mixtures using a broadly tunable swept external cavity quantum cascade laser," Analyst **142**(13), 2354–2362 (2017).
33. I. E. Gordon, L. S. Rothman, C. Hill, R. V. Kochanov, Y. Tan, P. F. Bernath, M. Birk, V. Boudon, A. Campargue, K. V. Chance, B. J. Drouin, J. M. Flaud, R. R. Gamache, J. T. Hodges, D. Jacquemart, V. I. Perevalov, A. Perrin, K. P. Shine, M. A. H. Smith, J. Tennyson, G. C. Toon, H. Tran, V. G. Tyuterev, A. Barbe, A. G. Csaszar, V. M. Devi, T. Furtenbacher, J. J. Harrison, J. M. Hartmann, A. Jolly, T. J. Johnson, T. Karman, I. Kleiner, A. A. Kyuberis, J. Loos, O. M. Lyulin, S. T. Massie, S. N. Mikhailenko, N. Moazzen-Ahmadi, H. S. P. Muller, O. V. Naumenko, A. V. Nikitin, O. L. Polyansky, M. Rey, M. Rotger, S. W. Sharpe, K. Sung, E. Starikova, S. A. Tashkun, J. Vander Auwera, G. Wagner, J. Wilzewski, P. Wcislo, S. Yu, and E. J. Zak, "The HITRAN2017 molecular spectroscopic database," J. Quant. Spectrosc. Radiat. Transfer **203**, 3–69 (2017).
34. S. W. Sharpe, T. J. Johnson, R. L. Sams, P. M. Chu, G. C. Rhoderick, and P. A. Johnson, "Gas-phase databases for quantitative infrared spectroscopy," Appl. Spectrosc. **58**(12), 1452–1461 (2004).
35. P. Werle, R. Mucke, and F. Slemr, "The limits of signal averaging in atmospheric trace-gas monitoring by tunable diode-laser absorption-spectroscopy (TDLAS)," Appl. Phys. B: Photophys. Laser Chem. **57**(2), 131–139 (1993).
36. J. D. Felix, E. M. Elliott, T. J. Gish, L. L. McConnell, and S. L. Shaw, "Characterizing the isotopic composition of atmospheric ammonia emission sources using passive samplers and a combined oxidation-bacterial denitrifier approach," Rapid Commun. Mass Spectrom. **27**(20), 2239–2246 (2013).

Optics EXPRESS

37. K. Sun, L. Tao, D. J. Miller, M. A. Zondlo, K. B. Shonkwiler, C. Nash, and J. M. Ham, "Open-path eddy covariance measurements of ammonia fluxes from a beef cattle feedlot," Agr. Forest Meteorol. **213**, 193–202 (2015).
38. L. Nugent-Glandorf, F. R. Giorgetta, and S. A. Diddams, "Open-air, broad-bandwidth trace gas sensing with a mid-infrared optical frequency comb," Appl. Phys. B: Lasers Opt. **119**(2), 327–338 (2015).